SIAM J. APPL. MATH.
Vol. 69, No. 2, pp. 552–564

STATISTICS OF POLARIZATION-MODE DISPERSION EMULATORS WITH UNEQUAL SECTIONS*

BRENTON R. STONE†, GINO BIONDINI‡, AND WILLIAM L. KATH§

Abstract. We study two models for the generation of polarization-mode dispersion (PMD) with unequal, fixed-length sections: an isotropic model, in which the orientations of all the sectional PMD vectors are taken to be randomly and uniformly varying across the Poincaré sphere, and a rotator model, in which all sections are taken to be linearly birefringent waveplates randomly rotatable with respect to one another. We describe the implementation of importance sampling for first- and second-order PMD in both models, including a targeting method for first-order PMD. We then use analytical and numerical methods to reconstruct the statistics of first- and second-order PMD for the two models. Our results show that the statistical properties of PMD depend significantly on the specific details of how PMD is generated.

Key words. optical fiber communications, Monte Carlo methods, importance sampling

AMS subject classifications. 65C05, 65C30, 78A10, 78A40, 78A48, 90B18

DOI. 10.1137/070696350

1. Introduction. Polarization-mode dispersion (PMD) is one of the major challenges facing the next generation of optical fiber communication systems [20]. Optical fiber is slightly birefringent due to slight deviations from circular symmetry, bending, stresses, etc. To first order in frequency, birefringence splits a pulse between the fast and the slow axes in an optical fiber; higher orders of birefringence induce depolarization and polarization-dependent chromatic dispersion. Also, the birefringence properties change randomly with distance, temperature, time, and wavelength, and these random variations are referred to as PMD. In system design, a certain power penalty is usually allotted to PMD, and one demands that the outage probability (the probability of the PMD-induced penalty exceeding this allowed value) be very small (typical requirements are a minute per year). Because of this stringent requirement, it has been difficult to use either Monte Carlo (MC) simulations or laboratory measurements to fully assess system outage probabilities, due to the extremely large number of PMD configurations that are necessary to obtain reliable estimates. Recently, it was shown that the technique of importance sampling (IS) [7, 8, 11] can often obviate this problem and allow efficient computation of PMD-induced transmission penalties and outage probabilities [6, 24, 25].

A measure of PMD is provided by the PMD vector [16]. The magnitude of the PMD vector, called differential group delay (DGD), quantifies the amount of local pulse splitting between fast and slow axes of birefringence. It has long been assumed that the probability density function (PDF) of the DGD follows a Maxwellian distribution [12], and that the process is ergodic, in the sense that time averages coincide

*Received by the editors July 5, 2007; accepted for publication (in revised form) July 29, 2008; published electronically December 3, 2008. This work was partially supported by the National Science Foundation under grants DMS-0406513 and DMS-0506101.

http://www.siam.org/journals/siap/69-2/69635.html

†Department of Mathematics, State University of New York, Buffalo, NY 14260 (brenton.stone@tyndall.af.mil). Current address: Applied Research Associates, Tyndall AFB, Panama City, FL 32403.

‡Department of Mathematics, State University of New York, Buffalo, NY 14260 (biondini@buffalo.edu).

§Department of Engineering Sciences and Applied Mathematics, Northwestern University, Evanston, IL 60208 (kath@northwestern.edu).

with frequency averages. Recent measurements of installed fiber links, however, have reported variations in the temporal statistics of DGD between different frequency channels in wavelength-division-multiplexed (WDM) systems [9, 19]. This more complicated behavior is consistent with a so-called hinge model of PMD [9], in which the system is composed of a concatenation of a small number of long, stable sections (long stretches of fiber which are buried underground) joined by short, unprotected sections, or "hinges" (bridges, amplifiers, service huts, etc.), which are more subject to environmental effects. While the hinges themselves bring little or no contribution to the total DGD of the system, their random fluctuations appear to be responsible for the temporal dynamics of PMD within each channel, whereas the longer sections appear to be essentially frozen in time. In the traditional model of PMD (which can be thought of as the limit in which the number of hinges is large and the stable sections are short), different wavelength bands behave independently but share the same statistical properties. In contrast, in the hinge model different wavelength bands are not statistically identical (because the individual PMD vector of each section is different for each wavelength). Thus, the ergodic hypothesis is not satisfied in the hinge model.

The properties of PMD in the hinge model have been well characterized [1, 2, 3, 10, 17, 21, 23, 26] under the assumption that the hinges randomize the orientation of the PMD vectors uniformly across the Poincaré sphere. In particular, analytical expressions for the PDF of the DGD are available [1, 17]. No analytical expressions exist, however, for the PDF of higher-order PMD, including second-order PMD. Moreover, some of the features of the hinge model also apply for different mechanisms of PMD generation that give rise to concatenations of fixed-length sections. No analytical expressions, however, are known for the statistics of PMD if one relaxes the assumption that the individual sections are uniformly distributed on the Poincaré sphere.

Here we address both of the above issues, and we discuss the PMD statistics produced by a finite concatenation of fixed-length sections for two specific PMD generation models. In the first model we take the orientation of the individual sections to be uniformly distributed on the Poincaré sphere. In the second model we take the individual sections to be linearly birefringent, with randomly oriented axes with respect to one another. We refer to the first and second models, respectively, as the "isotropic" and the "rotator" models of PMD. For both models, we study the case in which the individual section lengths are not all identical. Previously, we discussed the implementation of IS techniques for both models in the special case of equal-length sections [7, 8, 11]. Here we extend those results to the case of nonequal lengths, discussing the generation of large values of DGD, second-order PMD, as well as any combination of the two, plus a targeting method that allows one to concentrate samples where desired. Finally, we apply these methods to reconstruct PMD statistics of both models and show that significant differences exist among them.

2. Isotropic and rotator PMD models. The action of any lossless transmission element on an optical pulse can be described, up to a polarization-independent factor, by a unitary 2×2 frequency-dependent transmission matrix $U(z, \omega)$ called the Jones matrix, which describes the evolution of the transverse components of the optical field. Polarization effects can then be uniquely characterized by the real three-component PMD vector, $\vec{\tau}(\omega, z)$, defined by [16]

$$\vec{\tau}(\omega, z) \cdot \vec{\sigma} = 2i \frac{\partial U}{\partial \omega} U^{-1}, \tag{2.1}$$

where $\vec{\sigma}$ is a vector of Pauli matrices. Consider a concatenation a finite number of fixed-length fiber sections. The growth of PMD is governed, at each frequency, by the PMD concatenation equations. For first and second order, these are [16]

$$\vec{\tau}^{(n+1)} = \mathsf{R}_{n+1}\vec{\tau}^{(n)} + \Delta\vec{\tau}_{n+1}, \tag{2.2a}$$

$$\vec{\tau}_\omega^{(n+1)} = \mathsf{R}_{n+1}\vec{\tau}_\omega^{(n)} + \Delta\vec{\tau}_{n+1} \times \vec{\tau}^{(n+1)} + \Delta\vec{\tau}_{\omega,n+1}\,. \tag{2.2b}$$

Here $\vec{\tau}^{(n)}$ is the total PMD vector after the nth section, the fixed vector $\Delta\vec{\tau}_n$ is the PMD vector of the nth section, $\Delta\vec{\tau}_{\omega,n}$ is its frequency derivative, and the 3×3 matrix R_n is the Müller matrix of the nth section, which is related to the Jones matrix of that section by [16] $\mathsf{R}(\omega, z)\,\vec{\sigma} = U^{-1}\vec{\sigma}U$.

As is customary in both the traditional and the hinge model of PMD, we assume the sectional PMD vectors $\Delta\vec{\tau}_n$ to be constant in time and to have independent, identically distributed components that follow a normal distribution with mean zero and variance σ^2 with respect to wavelength. This of course implies that the sectional DGDs $\Delta\tau_n = |\Delta\vec{\tau}_n|$ are Maxwellian-distributed with respect to wavelength. Moreover, we assume that each section is linearly birefringent in frequency, namely, $\Delta\vec{\tau}_{\omega,n} = 0$. The matrix R_n then describes a rotation about an angle ϕ_n about the axis $\hat{r}_n = \Delta\vec{\tau}_n/|\Delta\vec{\tau}_n|$, namely,

$$\mathsf{R}_n = \exp\left[\phi_n\,\hat{r}_n\times\ \ \right] = \cos\phi_n\,\mathsf{I}_3 + (1-\cos\phi_n)\,\hat{r}_n\hat{r}_n^T + \sin\phi_n\,\hat{r}_n\times\ \ , \tag{2.3}$$

where I_3 is the 3×3 identity matrix and the superscript T denotes the matrix transpose. If hinges are present, a hinge rotation matrix H_n precedes R_{n+1} in (2.2).

In other words, mathematically there are two distinct random processes taking place. The first one governs the selection of the fiber sections, resulting in a set of wavelength-dependent sectional PMD vectors. These PMD vectors are stable over long periods of time (often months). The second random process is the one that governs the fast temporal variations due to environmental effects, and affecting the rotation angles in the matrices (2.3) as well as H_n. We model this situation by taking the section lengths to be fixed and by assuming that the only temporal variation in (2.2) arises from the rotation matrices R_{n+1} and, if present, from H_n. If the action of the hinges is sufficient to scatter the orientation of the PMD vectors uniformly across the Poincaré sphere, it is convenient to rewrite (2.2) as

$$\vec{\tau}^{(n+1)} = \mathsf{R}_{n+1}\mathsf{H}_n\big(\vec{\tau}^{(n)} + \Delta\vec{\tau}'_{n+1}\big), \tag{2.4a}$$

$$\vec{\tau}_\omega^{(n+1)} = \mathsf{R}_{n+1}\mathsf{H}_n\big(\vec{\tau}_\omega^{(n)} + \Delta\vec{\tau}'_{n+1}\times\vec{\tau}^{(n)}\big)\,, \tag{2.4b}$$

where $\Delta\vec{\tau}'_{n+1} = (\mathsf{R}_{n+1}\mathsf{H}_n)^{-1}\Delta\vec{\tau}_{n+1}$ is now uniformly distributed across the Poincaré sphere. We refer to this as the "isotropic" model of PMD. If one is interested only in first-order PMD, the problem is then equivalent to a 3-dimensional random walk. The DGD in the isotropic model and its impact on system behavior has been well characterized [1, 2, 3, 21, 26]. The isotropic hypothesis is a convenient assumption, since it makes an analytical treatment of the model possible. We emphasize, however, that it has not been experimentally validated, and that the question of whether or not it is accurate is an open issue.

When PMD is generated by birefringent waveplates, the individual PMD vectors lie on the equatorial plane of the Poincaré sphere. Since optical fiber is naturally linearly birefringent [14], the same statement holds for short fiber sections. Therefore, here we also consider the case in which the vectors $\Delta\vec{\tau}_{n+1}$ in (2.2) are uniformly

distributed on the equatorial plane of the Poincaré sphere. We refer to this as the "rotator" model of PMD. Of course, because the fiber birefringence axes change with distance, the concatenated total PMD vector will wander off the equatorial plane. Since the fiber correlation length (which is the distance over which the birefringence properties become uncorrelated) is below a hundred meters [15], any fiber span longer than a few kilometers will have a PMD vector that does not lie in the equatorial plane. (At the same time, however, significant nonuniformities in the angular distribution of PMD persist up to medium-to-long distances [28].) Note also that the rotator model neglects the action of the hinge rotation matrix. Thus it is an oversimplification of the actual PMD generation mechanism in installed systems.

Even though both of the above-mentioned fixed-length models may not be a fully accurate representation of the actual mechanism of PMD generation, in the absence of more complete models or conclusive experimental data the comparison between them will serve to demonstrate that the statistical properties of PMD depend significantly on the physical details of how PMD is generated in the system. (These results generalize those previously obtained for the case of equal-length sections [7, 11].)

The case of unequal-length sections has recently received renewed interest (e.g., see [17, 18, 26]), but only within the framework of the isotropic assumption. The case of unequal lengths is worthy of study because, while no analytical expressions exist for the PDF of the DGD (for the rotator model) or second-order PMD (for either model), most installed systems are composed of sections with unequal lengths. We also emphasize that a key assumption in both of the models considered here is that the individual sections have *fixed length*, namely, that the sectional PMD vectors are essentially frozen. A different model, in which the individual PMD vectors are also varying and in which, in particular, they are Maxwellian-distributed, was studied in [5, 22]. Note, however, that allowing the section lengths to vary on the same temporal scales as the rotation matrices results in very different PMD properties from those of the models considered here, even in the isotropic case (e.g., the PDF of the total DGD is exactly Maxwellian-distributed for any number of sections).

3. Importance sampling for unequal sections. Here we extend the IS methods that were derived in [7, 8, 11] for equal-length sections to the case of unequal section lengths, when the individual sections are either uniformly distributed on the Poincaré sphere or linearly birefringent. As mentioned previously, analytical expressions for the PDF of the DGD for the isotropic model are of course available both for equal and for unequal section lengths [1, 4, 17]. No similar expressions are known, however, when PMD is generated by birefringent waveplates. Moreover, no analytic expressions are known for the PDF of second-order PMD in either model. It was shown [24] that in systems which employ PMD compensation, knowledge of first-order PMD is not enough to accurately characterize PMD-induced transmission penalties. At the same time, it has also been shown that control of both first- and second-order PMD is enough in most cases of interest [24]. Finally, we should note that one of the advantages of IS is that, whether one is biasing for first- or second-order PMD, the method automatically generates PMD of all orders (due to the wavelength dependence of the sectional PMD vectors). This means that biasing for large DGDs can also be useful in the isotropic model (even though the PDF of the DGD is known), since the simultaneous presence of all orders of PMD can lead to a more accurate evaluation of PMD-induced distortions [24].

3.1. IS for the DGD. The first step when applying IS is to determine the most likely system configurations that lead to the event of interest. For first-order PMD, this proceeds exactly in the same way as in the case of equal-length sections [7]. Namely, one must choose the next PMD contribution $\Delta\vec{\tau}_{n+1}$ to be preferentially aligned with the previous PMD vector $\vec{\tau}^{(n)}$. For the isotropic model, this is done choosing the angle θ_n between $\Delta\vec{\tau}_{n+1}$ and $\vec{\tau}^{(n)}$ to be preferentially close to 0. For the rotator model, instead, since $\Delta\vec{\tau}_{n+1}$ must lie in the equatorial plane of the Poincaré sphere, the biasing is done by choosing the angle θ_n between $\Delta\vec{\tau}_{n+1}$ and the projection of $\vec{\tau}^{(n)}$ onto the equatorial plane to be preferentially close to 0.

To achieve this preferential alignment, for the isotropic model we take $\cos\theta = 2x^{1/\alpha} - 1$, while for the rotator model we take $\theta = \pi\ \mathrm{sgn}(2x-1)|2x-1|^{\alpha}$, in both cases with x uniform in $[0,1]$. These choices correspond respectively to the biasing distributions

$$p_{\alpha,\mathrm{iso}}(\theta) = (\alpha/2)\sin\theta\,[(1+\cos\theta)/2]^{\alpha-1}, \qquad p_{\alpha,\mathrm{wav}}(\theta) = (1/\alpha\pi)\,|\theta/\pi|^{1-\alpha}. \tag{3.1}$$

For both the isotropic and the rotator models the value $\alpha = 1$ reproduces the unbiased case, while larger values of α concentrate the samples θ near 0. In both models, the likelihood ratio is given by [8]

$$L(\theta_1,\ldots,\theta_N) = \prod_{n=1}^{N} \frac{p_1(\theta_n)}{p_\alpha(\theta_n)}\,, \tag{3.2}$$

where N is the total number of sections. Of course, other choices of biasing distributions might work equally well, as long as the reference angles are correctly identified. Also, in both models the rotation angle ϕ_n is not important for IS purposes, and is taken to be varying and uniformly distributed in $[0, 2\pi]$.

3.2. IS for first- and second-order PMD. Consider the orthogonal frame of reference defined by the unit vectors

$$\hat{u}_1^{(n)} = \vec{\tau}^{(n)}/|\vec{\tau}^{(n)}|\,, \qquad \hat{u}_2^{(n)} = \vec{\tau}_{\omega,\perp}^{(n)}/|\vec{\tau}_{\omega,\perp}^{(n)}|\,, \qquad \hat{u}_3^{(n)} = \hat{u}_1^{(n)} \times \hat{u}_2^{(n)}\,, \tag{3.3}$$

where $\vec{\tau}_{\omega,\parallel}$ and $\vec{\tau}_{\omega,\perp}$ are, respectively, the parallel and perpendicular components of $\vec{\tau}_\omega$ with respect to τ. As in [8], it is convenient to consider the continuum limit of (2.2). In the isotropic model, factoring out the inessential rotation $\mathsf{R}_{n+1}\mathsf{H}_n$ in (2.4), one then obtains

$$\frac{d\tau}{dz} = b_1\,, \qquad \frac{d\tau_{\omega,||}}{dz} = b_2\,\frac{\tau_{\omega,\perp}}{\tau}\,, \qquad \frac{d\tau_{\omega,\perp}}{dz} = b_3\tau - b_2\,\frac{\tau_{\omega,||}}{\tau}\,, \tag{3.4}$$

where $\vec{b}(z) = \lim_{\Delta z\to 0}\Delta\vec{\tau}_{n+1}/\Delta z$ quantifies the rate at which PMD is added, and (b_1, b_2, b_3) are the components of $\vec{b}$ with respect to the reference frame $\{\hat{u}_1, \hat{u}_2, \hat{u}_3\}$.

As shown in [8], (3.4) can be solved exactly for any $\vec{b}(z)$. One can then use calculus of variations to find the choice of $\vec{b}(z)$ which maximizes second-order PMD. In the case of equal-length sections, that is, $|\vec{b}(z)| = b = \mathrm{const}$, it was shown in [11] that the solution of this maximization problem is

$$\vec{b}(z) = b\,\big(\hat{u}_1\,\cos[\Phi(z)] + \hat{u}_3\,\sin[\Phi(z)]\big), \tag{3.5}$$

where the biasing angle is $\Phi(z) = (z/z_{\max})\Phi_{\max}$ and where $\Phi_{\max} = \pi/2$. Other choices of $\Phi_{\max}$ maximize linear combinations of DGD and second-order PMD ($\Phi_{\max} = 0$ is simply first-order biasing).

As we show next, the solution of the maximization problem in the case of unequal section lengths can be obtained from the case of equal section lengths by a simple change of variable. Given a function $b(z) = |\vec{b}(z)|$ that describes the magnitude of the local birefringence, define the rescaled distance

$$\zeta(z) = \int_0^z b(z')dz' \,. \tag{3.6}$$

Written in terms of ζ, equations (3.4) then are

$$\frac{d\tau}{d\zeta} = e_1 \,, \qquad \frac{d\tau_{\omega,||}}{d\zeta} = e_2 \, \frac{\tau_{\omega,\perp}}{\tau} \,, \qquad \frac{d\tau_{\omega,\perp}}{d\zeta} = e_3\tau - e_2 \, \frac{\tau_{\omega,||}}{\tau} \,, \tag{3.7}$$

where $\hat{e}(z) = \vec{b}(z)/|\vec{b}(z)|$ has unit magnitude. One can now use the results of the calculations for equal-length sections described above, obtaining

$$\hat{e}(\zeta) = \hat{u}_1 \, \cos[\Phi(\zeta)] + \hat{u}_3 \, \sin[\Phi(\zeta)] \,, \tag{3.8}$$

with $\Phi(\zeta) = (\zeta/\zeta_{\max}) \, \Phi_{\max}$. In terms of the original variable z one then obtains (3.5), with b replaced by $b(z)$ and where now

$$\Phi(z) = \Phi_{\max} \int_0^z b(z')dz' \Big/ \int_0^{z_{\max}} b(z')dz' \,, \tag{3.9}$$

with the same meaning for $\Phi_{\max}$. (Of course, (3.9) reduces to the linearly varying profile (3.10) in the case of equal section lengths.) In the discrete version, with section lengths $\Delta\tau_n$, we then obtain Φ_n, which gives the proper biasing direction after n sections as a function of n:

$$\Phi_n = \Phi_{\max} \sum_{m=1}^{n} \Delta\tau_m/\tau_{\max}, \tag{3.10}$$

where

$$\tau_{\max} = \sum_{n=1}^{N} \Delta\tau_n \,. \tag{3.11}$$

As with the DGD, the biasing directions for the rotator model are just the projection of the vector $\vec{b}$ onto the equatorial plane. Moreover, once the deterministic biasing directions have been found, for both the isotropic and the rotator model, one selects the biasing distributions in order to concentrate the MC samples around the deterministic biasing directions exactly as when biasing for the DGD. When more than one choice of biasing is necessary, multiple IS can be used, and samples from different biasing distributions can be combined using the balance heuristic [8].

3.3. Targeted IS. It is sometimes useful to be able to choose where to concentrate the MC samples, especially when one is interested in only a small region of the PDF. We now obtain an estimate of the values of the biasing strength α that are needed to generate values of DGD concentrated near a given target.

A simple bound on α can be obtained by looking at the component of the next PMD vector, $\tau^{(n+1)}$, that is parallel to the previous PMD vector, $\tau^{(n)}$. From (2.4a) it is

$$\tau_{||}^{(n+1)} = \tau^{(n)} + \Delta\tau_{n+1} \cos\theta_{n+1}, \tag{3.12}$$

where θ_{n+1} is the angle between the differential contribution of the next section, $\Delta\tau_{n+1}$, and the previous PMD vector. Since it is obviously true that $|\vec{\tau}^{(n)}| \geq |\tau_{||}^{(n)}|$, from (3.12) we have

$$\tau_{||}^{(N)} \geq \sum_{n=1}^{N} \Delta\tau_n \cos\theta_n. \tag{3.13}$$

Then, since the section lengths are fixed, taking expectation values we have

$$\langle\tau^{(N)}\rangle \geq \sum_{n=1}^{N} \Delta\tau_n \langle\cos\theta_n\rangle = \langle\cos\theta\rangle\, \tau_{\max}\,, \tag{3.14}$$

where we used $\langle\tau^{(N)}\rangle \geq \langle\tau_{||}^{(N)}\rangle$, and where $\tau_{\max}$ is the maximum DGD, defined in (3.11). For the biased probability distribution for the isotropic model, (3.1), it is

$$\langle\cos\theta\rangle = (\alpha-1)/(\alpha+1). \tag{3.15}$$

Therefore in this case (3.14) yields

$$\langle\tau^{(N)}\rangle \geq [(\alpha-1)/(\alpha+1)]\, \tau_{\max}\,. \tag{3.16}$$

Note that as α increases, $\langle\tau^{(N)}\rangle$ approaches $\tau_{\max}$, as expected.

Equation (3.16) yields an upper bound on the value of the biasing parameter α that is necessary to obtain samples distributed near $\langle\tau^{(N)}\rangle = \tau_{\text{target}}$, namely, $\alpha_{\text{target}} \leq \alpha_o$, where

$$\alpha_o = (\tau_{\max} + \tau_{\text{target}})/(\tau_{\max} - \tau_{\text{target}})\,. \tag{3.17}$$

Note, however, that the above result is only an upper bound, and the actual value of α_{target} that concentrates the samples around a desired target is often a great deal smaller than α_o, particularly if $\tau_{\max} - \tau_{\text{target}}$ is small. In those cases, the heuristic correction $\alpha = \alpha_o/\sqrt{1+\alpha_o/4}$, where α_o is given by (3.17), provides a better estimate of α_{target} which is valid over the whole range of DGDs.

The bound on α_{target} is independent of the particular values of the section lengths, and therefore it holds equally well for equal as well as unequal lengths. Moreover, it also appears to hold for the rotator model. It should be noted that for PMD generation models in which the section lengths are also variable and are Maxwellian-distributed, one could also concentrate the samples around a target value of second-order PMD [5]. Note also that, using the so-called Brownian bridge method, one could hit exactly any value of DGD [27]. To the best of our knowledge, however, no targeting method was known for fixed-length sections.

4. Numerical simulations and PMD statistics. We now proceed to compare statistical measures of PMD for the isotropic and the rotator models of PMD defined in section 2, using the methods discussed in section 3.

4.1. PDF of the DGD. An exact formula for the PDF of the DGD in the isotropic model, hereafter $p_{\text{DGD}}(\tau)$, was obtained in [1]. That expression, however, involves a sum over 2^N terms, where as before N is the number of sections. Hence, the computational cost of evaluating it increases exponentially with N. As a result,

the use of that formula is impractical except for very small values of N. Fortunately, an alternative exact expression exists for the PDF of the DGD, in terms of a Fourier sine series [4]:

$$p_{\mathrm{DGD}}(\tau) = \frac{2\pi\tau}{\tau_{\max}^2} \sum_{m=1}^{\infty} m \sin\left(\frac{m\pi\tau}{\tau_{\max}}\right) \prod_{n=1}^{N} \frac{\sin(m\pi\Delta\tau_n/\tau_{\max})}{m\pi\Delta\tau_n/\tau_{\max}}\,. \tag{4.1}$$

The evaluation of (4.1) is of course always affected by truncation error due to the finite number of Fourier modes. Nonetheless, (4.1) produced the same results as the formula in [1] up to roundoff error in all the cases we tested (which included situations where the DGD of one section is larger than the sum of all the others). In our tests the two methods had about the same execution time for $N = 6$ sections when 2^{10} Fourier modes were used in (4.1). The computational cost of evaluating (4.1), however, is essentially given by the number of Fourier modes used, and depends only very weakly on the number of sections [23]. For this reason we used (4.1) in our calculations. For the rotator model one must use importance-sampled MC (IS-MC) simulations as discussed in section 3.1, using a combination of biasing strengths, to cover the whole range of DGDs. The PDF of the DGD is then reconstructed from the IS-MC simulations using the likelihood ratios as described in [8].

Figure 4.1 shows the PDF of the DGD for the isotropic model (thick dashed line) and the rotator model (thick solid line) for two particular realizations of $N = 8$ section lengths, while Figure 4.2 shows the PDF of the DGD for a specific realization of $N = 20$ sections. The specific values of the sectional DGDs are given in Table 4.1; the corresponding values of $\tau_{\max}$ are, respectively, 10.99 ps, 16.19 ps, and 21.60 ps for cases A, B, and C. In each case, the sectional DGDs were all drawn from an identical Maxwellian distribution

$$p_{\mathrm{dgd}}(\tau) = \frac{\sqrt{2}\,\tau^2}{\sqrt{\pi}\,\sigma^3}\, e^{-\tau^2/2\sigma^2}\,, \tag{4.2}$$

where $\sigma^2 = (\pi/8)\langle\Delta\tau\rangle^2$. In particular, we set $\langle\Delta\tau\rangle = \langle\tau\rangle/\sqrt{N}$ with $\langle\tau\rangle = 5\,\mathrm{ps}$ in all cases, so as to obtain a nominal Maxwellian distribution with mean DGD of 5 ps for the whole line. Note, however, that due to the finite sample size (i.e., the finite value of N), the samples will generate a PDF of the DGD which is better approximated by an "effective" Maxwellian, obtained by (4.2) with $\sigma_{\mathrm{eff}}^2 = (\pi/8)\sum_{n=1}^{N}(\Delta\tau_n)^2$. These effective Maxwellian distributions are shown in Figure 4.1 as dot-dashed lines. Of course the difference between the nominal and effective Maxwellians will tend to zero on average as N goes to infinity.

For the rotator model we used the biasing strengths $\alpha = 1$ (unbiased), 4, 12, and 24 to perform IS-MC simulations in the cases with $N = 8$, and we used $\alpha = 1$, 2, 4, and 6 in the case $N = 20$ (since in this case smaller biasing strengths are sufficient to cover the desired range of values of the PDF). In all cases 400,000 samples per biasing strength were used. Note how, in all cases, the tails of the PDF for the isotropic model (that is, the values of the PDF for values of DGD near $\tau_{\max}$) are orders of magnitudes below those of the rotator model. This behavior occurred in all cases we studied, but it is not clear at present whether it is a general property, namely, whether it holds for any choice of section lengths and for any number of sections (as is indeed the case with equal lengths). As is to be expected, the PDF in the case of $N = 20$ sections agrees with a Maxwellian distribution over a larger range of DGDs.

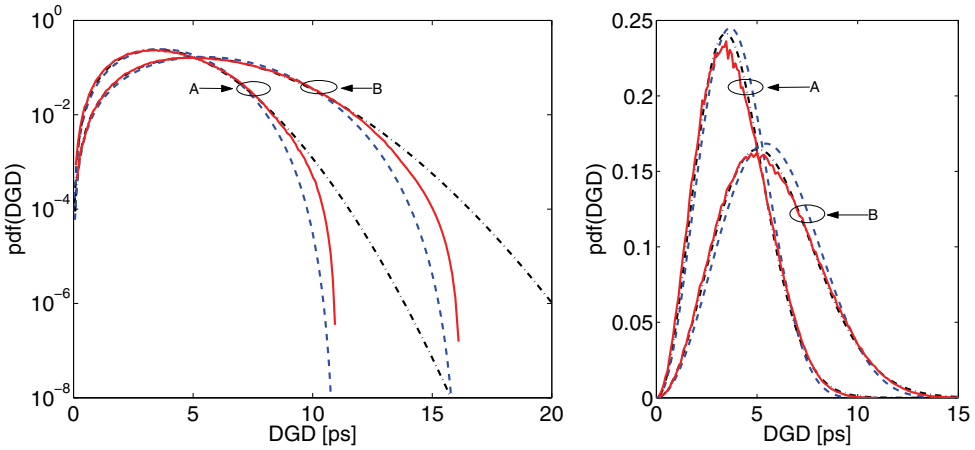

FIG. 4.1. *PDF of the DGD for a concatenation of $N = 8$ sections, for two particular choices of individual section DGDs drawn from an identical Maxwellian distribution with mean $5/\sqrt{N}$ ps (cases* A *and* B *in Table* 4.1*). Dashed lines: isotropic model; solid lines: rotator model. The dot-dashed lines show the effective Maxwellian distribution. Left: logarithmic scale; right: linear scale.*

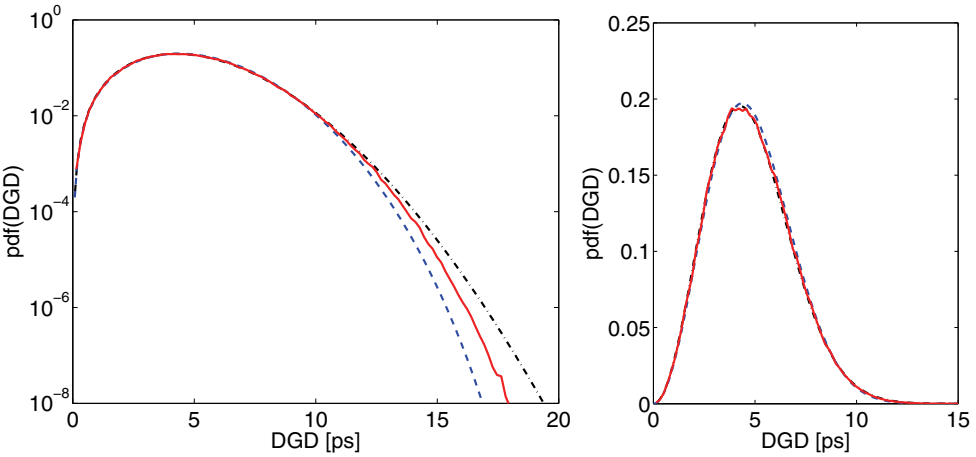

FIG. 4.2. *Same as Figure* 4.1*, but for a concatenation of $N = 20$ sections drawn from a Maxwellian distribution with mean $5/\sqrt{N}$ ps (case* C *in Table* 4.1*).*

TABLE 4.1
Sectional DGDs (in ps) used in the MC simulations.

A		1.149	2.077	1.390	2.094	1.260	0.2761	1.812	0.9307	
B		1.632	2.278	1.678	3.584	2.034	0.948	1.164	2.868	
C	1.170	1.624	0.554	1.127	1.232	0.450	0.916	0.589	1.094	1.236
	1.230	0.824	1.243	0.997	0.511	0.628	1.397	1.853	0.841	2.089

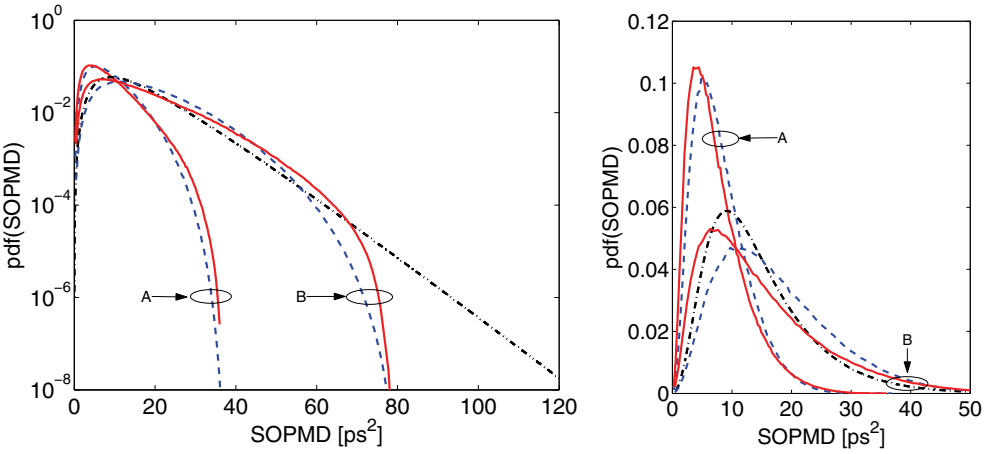

FIG. 4.3. *PDF of second-order PMD (SOPMD) for the same section DGDs as in Figure* 4.1. *Dashed lines: isotropic model; solid lines: rotator model. The dot-dashed line shows a sech-tanh distribution with* $\langle\tau\rangle = 5$ *ps. Left: logarithmic scale; right: linear scale.*

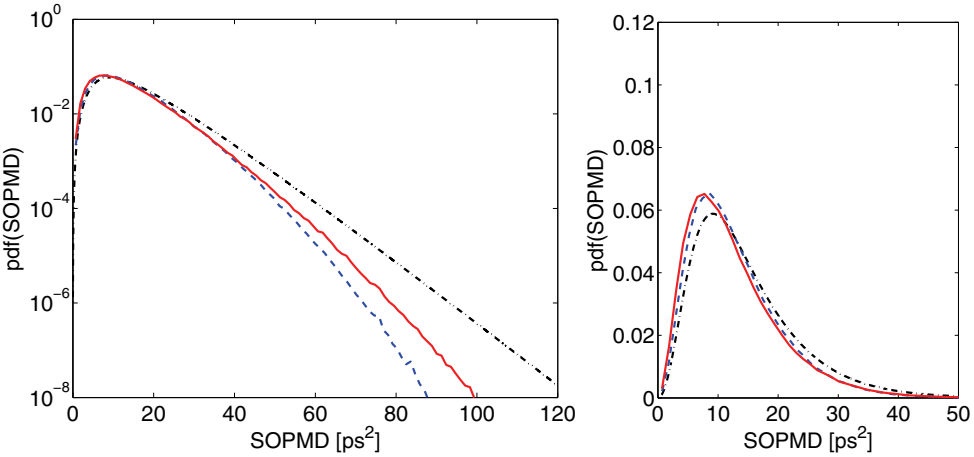

FIG. 4.4. *Same as Figure* 4.3, *but for* $N = 20$ *and with the same section DGDs as in Figure* 4.2.

4.2. PDF of second-order PMD. No analytical solutions exist for the PDF of second-order PMD generated by a concatenation of a finite number of fixed-length sections, even in the isotropic case and even in the case of equal-length sections. Therefore, one must resort to numerical simulations for both the isotropic and the rotator model. We used IS-MC simulations as discussed in section 3.2 with $\Phi_{\max} = \pi/2$, again with a combination of biasing strengths to cover the whole range of second-order PMD. More precisely, we used the same values of biasing strength as when biasing for large values of DGD.

Figure 4.3 shows the PDF of second-order PMD for the isotropic and the rotator model for the same section lengths as in Figure 4.1, while Figure 4.4 does the same for the same section lengths as in Figure 4.2. In all cases the solid line shows the nominal

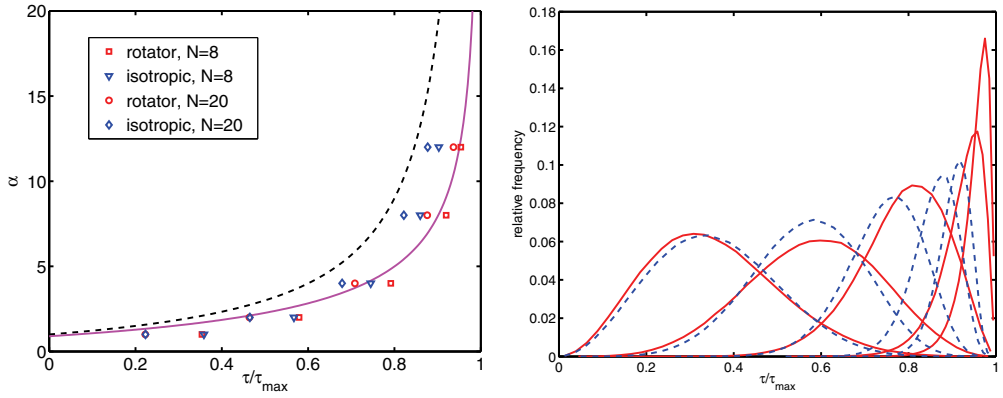

FIG. 4.5. *Left: The estimated value of the biasing strength needed to obtain a given fraction of the maximum DGD. Dashed line: uncorrected value; solid line: value with the heuristic correction. Also shown are the means of the biased MC samples obtained with the biasing strengths* $\alpha = 1, 2, 4, 8, 12$ *for both the isotropic and the rotator model with* $N = 8$ *and* $N = 20$. *Right: The relative frequency of the total DGD obtained with the biasing values for* $N = 8$ *in the isotropic model (dashed curves) and the rotator model (solid curves) in case* A.

"sech-tanh" distribution obtained in the limit of large number of sections [13], namely,

$$p_{\mathrm{sopmd}}(x) = \frac{8}{\pi \langle \tau \rangle^2}\, y(x)\, \mathrm{sech}[y(x)]\, \tanh[y(x)]\,, \tag{4.3}$$

where $y(x) = 4x/\langle \tau \rangle^2$. For both the isotropic and the rotator model, the simulations were done with the same biasing strengths as for the DGD, with 200,000 samples per biasing strength for both models. As with the DGD, the tails of the PDF of the rotator model are significantly larger than those of the isotropic model. (The maximum second-order PMD for an isotropic concatenation of sections was obtained in [18].) Here, however, the difference between the two models seems to be less pronounced than for the PDF of the DGD.

It should be clear from the figures that the overall PDFs of both DGD and second-order PMD can depend significantly on how much of the Poincaré sphere is being sampled by the hinge rotation matrix. It should also be clear that since the maximum DGD and maximum second-order PMD of any PMD emulator are determined by the particular values of the individual DGDs, the resulting PDFs can vary quite a bit for different choices of the section DGDs, even though the individual DGDs are all drawn from an identical Maxwellian distribution. In particular, these PDFs can occasionally differ significantly from the average Maxwellian and sech-tanh distributions, even at moderate values of DGD and second-order PMD, and even with a relatively large number of sections. This is indeed evident from Figures 4.1 and 4.3.

4.3. Targeting. Figure 4.5 shows (to the left) a comparison of the estimate (3.17) of the biasing strength α_o (dashed line) required to obtain a given target DGD versus the heuristic correction α (solid line). Both are plotted against the normalized total DGD (namely, the ratio $\tau/\tau_{\max}$). Also plotted is the mean of the biased MC samples obtained for both the isotropic and the rotator model with $\alpha = 1$ (unbiased), 2, 4, 8, and 12, computed for both $N = 8$ and $N = 20$ with the section lengths listed in Table 4.1. (The results from cases A and B are indistinguishable from each other.) As is evident from this comparison, a good agreement exists between the analytical

approximation and the actual mean of the MC samples for both the isotropic and the rotator model for values of N up to 20, except for small values of α. (For $\alpha = 1$, (3.17) yields the unphysical value $\langle\tau\rangle = 0$.) Note, however, that the agreement becomes worse for larger values of N. This is to be expected, since $\langle\tau\rangle/\tau_{\max} \to 0$ in the limit $N \to \infty$, even when the mean DGD per section is scaled as $\langle\tau\rangle/\sqrt{N}$ so as to keep $\langle\tau\rangle$ fixed.

Also shown (to the right) are histograms showing the expected relative frequency of the values of total DGD (as estimated from biased MC simulations) for case A for both the isotropic (dashed lines) and the rotator (solid lines) models for the same values of α as above, illustrating how the IS-MC samples indeed cluster around the expected mean for both the isotropic and the rotator model.

5. Conclusions. We have discussed two models of PMD generation, both consisting of a concatenation of unequal-length sections: a conventional, isotropic model, based on the assumption that the action of the hinges connecting the individual fiber sections causes their relative orientations to vary uniformly across the Poincaré sphere; and a rotator model, based on linearly birefringent elements that rotate relative to one another. We have presented the implementation of IS for both the isotropic model and the rotator model with sections of arbitrary length, and we have used analytical and numerical methods to compute the statistics of first- and second-order PMD in both models. The results show that the PMD statistics depend significantly upon the details of how PMD is generated.

We should reiterate that even though only first- and second-order PMD are biased, a full range of higher-order PMD is also being generated. Moreover, it has been shown [24] that multiple IS with a proper choice of biasing strengths which cover the whole (DGD, second-order PMD) plane is sufficient to accurately capture the statistical distribution of PMD-induced transmission penalties even when multistage PMD compensators are used and even when first-order and second-order PMD are completely compensated.

Thus, the present methods can be employed to compute PMD-induced pulse distortions in systems with various configurations. The present work also provides a further demonstration that the PMD-induced penalties depend on the specific physical details of how PMD is generated in the system. More specifically, for the hinge model they depend on how much of the Poincaré sphere is sampled by the hinge rotation matrix. If the actual PMD generation mechanism in some realistic situation can be considered to be a hybrid between the isotropic and the rotator models, these two models could then provide useful upper and lower limits for the actual penalties in the system.

Acknowledgment. We thank H. Kogelnik and P. J. Winzer for many insightful discussions.

REFERENCES

[1] C. Antonelli and A. Mecozzi, *Statistics of the DGD in PMD emulators*, IEEE Photon. Technol. Lett., 16 (2004), pp. 1804–1806.
[2] C. Antonelli and A. Mecozzi, *Theoretical characterization and system impact of the hinge model of PMD*, J. Lightwave Technol., 24 (2006), pp. 4064–4074.
[3] C. Antonelli, A. Mecozzi, K. Cornick, M. Brodsky, and M. Boroditsky, *PMD-induced penalty statistics in fiber links*, IEEE Photon. Technol. Lett., 17 (2005), pp. 1013–1015.
[4] R. Barakat, *Isotropic random flights*, J. Phys. A, 6 (1973), pp. 796–804.
[5] G. Biondini and W. L. Kath, *PMD emulation with Maxwellian length sections and importance sampling*, IEEE Photon. Technol. Lett., 16 (2004), pp. 789–791.

[6] G. Biondini and W. L. Kath, *Polarization-dependent chromatic dispersion and its impact on return-to-zero transmission formats*, IEEE Photon. Technol. Lett., 17 (2005), pp. 1866–1868.

[7] G. Biondini, W. L. Kath, and C. R. Menyuk, *Importance sampling for polarization-mode dispersion*, IEEE Photon. Technol. Lett., 14 (2002), pp. 310–312.

[8] G. Biondini, W. L. Kath, and C. R. Menyuk, *Importance sampling for polarization mode dispersion: Techniques and applications*, IEEE J. Lightwave Technol., 22 (2004), pp. 1201–1215; errata, 24 (2006), p. 1065.

[9] M. Brodsky, M. Boroditsky, P. Magill, N. J. Frigo, and M. Tur, *Persistence of spectral variations in DGD statistics*, Opt. Expr., 13 (2005), pp. 4090–4095.

[10] M. Brodsky, N. J. Frigo, M. Boroditsky, and M. Tur, *Polarization-mode dispersion of installed fibers*, IEEE J. Lightwave Technol., 17 (2006), p. 4584.

[11] S. L. Fogal, G. Biondini, and W. L. Kath, *Multiple importance sampling for first- and second-order polarization mode dispersion*, IEEE Photon. Technol. Lett., 14 (2002), pp. 1273–1275; errata, 14 (2002), p. 1487.

[12] G. J. Foschini and C. D. Poole, *Statistical theory of polarization dispersion in single mode fibers*, IEEE J. Lightwave Technol., 9 (1991), pp. 1439–1456.

[13] G. J. Foschini, L. E. Nelson, R. M. Jopson, and H. Kogelnik, *Probability densities of second-order polarization-mode dispersion including polarization-dependent chromatic dispersion*, IEEE Photon. Technol. Lett., 12 (2000), pp. 293–295.

[14] A. Galtarossa, L. Palmieri, M. Schiano, and T. Tambosso, *Statistical characterization of fiber random birefringence*, Opt. Lett., 25 (2000), pp. 1322–1324.

[15] A. Galtarossa, L. Palmieri, M. Schiano, and T. Tambosso, *Measurements of birefringence correlation length in long single-mode fibers*, Opt. Lett., 26 (2001), p. 962.

[16] J. P. Gordon and H. Kogelnik, *PMD fundamentals: Polarization-mode dispersion in optical fibers*, Proc. Natl. Acad. Sci., 97 (2000), pp. 4541–4550.

[17] M. Karlsson, *Probability density functions of the differential group delay in optical fiber communication systems*, IEEE J. Lightwave Technol., 19 (2001), pp. 324–331.

[18] M. Karlsson, *Geometric interpretation of second-order PMD*, IEEE J. Lightwave Technol., 26 (2006), pp. 643–651.

[19] M. Karlsson, J. Brentel, and P. A. Andrekson, *Long-term measurement of PMD and polarization drift in installed fibers*, J. Lightwave Technol., 18 (2000), pp. 941–951.

[20] H. Kogelnik, L. E. Nelson, and R. M. Jopson, *Polarization mode dispersion*, in Optical Fiber Telecommunications IVB, I. P. Kaminow and T. Li, eds., Academic Press, San Diego, CA, 2002, pp. 725–861.

[21] H. Kogelnik, P. Winzer, L. E. Nelson, R. M. Jopson, M. Boroditsky, and M. Brodsky, *First-order PMD outage for the hinge model*, IEEE Photon. Technol. Lett., 17 (2005), pp. 1208–1210; errata, 17 (2005), p. 2499.

[22] J. H. Lee, M. S. Kim, and Y. C. Chung, *Statistical PMD emulator using variable DGD elements*, IEEE Photon. Technol. Lett., 15 (2003), pp. 54–56.

[23] J. Li, G. Biondini, H. Kogelnik, and P. J. Winzer, *Noncompliant capacity ratio for systems with an arbitrary number of polarization hinges*, IEEE J. Lightwave Technol., 26 (2008), pp. 2110–2117.

[24] A. O. Lima, C. R. Menyuk, and I. T. Lima, *Comparison of two biasing Monte Carlo methods for calculating outage probabilities in systems with multisection PMD compensators*, IEEE Photon. Technol. Lett., 17 (2005), pp. 2580–2582.

[25] I. T. Lima, Jr., A. O. Lima, G. Biondini, C. R. Menyuk, and W. L. Kath, *A comparative study of single-section polarization-mode dispersion compensators*, IEEE J. Lightwave Technol., 22 (2004), pp. 1023–1032.

[26] A. Mecozzi, C. Antonelli, M. Boroditsky, and M. Brodsky, *Characterization of the time dependence of polarization mode dispersion*, Opt. Lett., 29 (2004), pp. 2599–2601.

[27] M. Shtaif, *The Brownian-bridge method for simulating polarization mode dispersion in optical communications systems*, IEEE Photon. Technol. Lett., 15 (2003), pp. 51–53.

[28] Y. Tan, J. Yang, W. L. Kath, and C. R. Menyuk, *Transient evolution of the polarization-dispersion vector's probability distribution*, J. Opt. Soc. Amer. B, 19 (2002), pp. 992–1000.